Application of a novel porous tantalum implant in rabbit anterior lumbar spine fusion model: *in vitro* and *in vivo* experiments

Ming Lu[1,2], Song Xu[3], Zi-Xiong Lei[1,2], Dong Lu[4], Wei Cao[5], Marko Huttula[5], Chang-He Hou[1,2], Shao-Hua Du[1,2], Wei Chen[1,2], Shuang-Wu Dai[1,2], Hao-Miao Li[1,2], Da-Di Jin[1,2]

[1]Department of Orthopedic, The Third Affiliated Hospital of Southern Medical University, Guangzhou, Guangdong 510630, China;

[2]Academy of Orthopaedics of Guangdong Province, Guangzhou, Guangdong 510630, China;

[3]Department of Arthroplasty, Nanfang Hospital, Southern Medical University, Guangzhou, Guangdong 510515, China;

[4]Ning Xia Orient Tantalum Industry Co. Ltd, Shizuishan, Ningxia 753000, China;

[5]Department of Physics, University of Oulu, Oulu FIN-90014, Finland.

Abstract

Background Some porous materials have been developed to enhance biologic fusion of the implants to bone in spine fusion surgeries. However, there are several inherent limitations. In this study, a novel biomedical porous tantalum was applied to *in vitro* and *in vivo* experiments to test its biocompatibility and osteocompatibility.

Methods Bone marrow-derived mesenchymal stem cells (BMSCs) were cultured on porous tantalum implant. Scanning electron microscope (SEM) and Cell Counting Kit-8 assay were used to evaluate the cell toxicity and biocompatibility. Twenty-four rabbits were performed discectomy only (control group), discectomy with autologous bone implanted (autograft group), and discectomy with porous tantalum implanted (tantalum group) at 3 levels: L3–L4, L4–L5, and L5–L6 in random order. All the 24 rabbits were randomly sacrificed at the different post-operative times (2, 4, 6, and 12 months; n = 6 at each time point). Histologic examination and micro-computed tomography scans were done to evaluate the fusion process. Comparison of fusion index scores between groups was analyzed using one-way analysis of variance. Other comparisons of numerical variables between groups were made by Student *t* test.

Results All rabbits survived and recovered without any symptoms of nerve injury. Radiographic fusion index scores at 12 months post-operatively between autograft and tantalum groups showed no significant difference (2.89 ± 0.32 vs. 2.83 ± 0.38, $F = 244.60$, $P = 0.709$). Cell Counting Kit-8 assay showed no significant difference of absorbance values between the leaching liquor group and control group (1.25 ± 0.06 vs. 1.23 ± 0.04, $t = -0.644$, $P = 0.545$), which indicated the BMSC proliferation without toxicity. SEM images showed that these cells had irregular shapes with long spindles adhered to the surface of tantalum implant. No implant degradation, wear debris, or osteolysis was observed. Histologic results showed solid fusion in the porous tantalum and autologous bone implanted intervertebral spaces.

Conclusion This novel porous tantalum implant showed a good biocompatibility and osteocompatibility, which could be a valid biomaterial for interbody fusion cages.

Keywords: Porous tantalum; anterior lumbar interbody fusion; bone ingrowth; chemical vapor deposition; three-dimensional knitted framework

Introduction

Spine fusion has become a routine technique in the field of spine surgery, and has been widely used in the treatment of lumbar spine degeneration, cervical spine instability, intervertebral disc injury, and spinal deformity. Generally speaking, the spinal fusion surgery is an effective method to achieve spinal stability and nerve decompression.[1] However, it is usually associated with a high incidence of fusion failure and pseudarthrosis (5–35%). Two of the most important factors are bone grafting materials and bone transplantation mode selection.[2]

The development of spinal surgery has put forward higher requirements for bone implants. With the development of new technologies and new materials, more and more new bone substitutes, which meet the biomechanical character-

---

Access this article online

Quick Response Code:

Website:
www.cmj.org

DOI:
10.1097/CM9.0000000000000030

---

istics of human body, emerged as the times require.[3-8] The ideal bone substitute materials should have the characteristics of bone conduction, bone induction, no immunogenicity, no risk of disease transmission, suitable mechanical strength, cost-effective, and easy to use. So far autologous bone is still the best material for intervertebral fusion. However, it is limited by some of the disadvantages of autologous bone, including additional surgical trauma, increased risk of post-operative complications such as infections, hematomas, and pain in donor-site, and limited supply of autologous bone.[9-12] The use of allogeneic and xenogeneic bone is also likely to bring risks such as immune rejection and bone disease spread.[13,14] The calcium-based and polymeric artificial bone substitutes have been plagued by problems such as poor biodegradability, biocompatibility, and biomechanics so as to lead a low fusion rate.[15,16] Therefore, a material with good biocompatibility, bone conduction, and even induction of bone ingrowth, which can be used to improve the rate of spinal fusion and bone regeneration, has become a hot research topic.

In the past 30 years, it has witnessed a fast development in the medical porous materials which have been substituting solid metals in bone implantation surgeries. Compared with solid implant metals, the porous ones advance in lighter weight, larger contact surfaces, as well as closer mechanic properties to the human bones. Porous tantalum has been proved to be one of the most suitable substitution materials for human bone due to its similar structure and mechanic properties as human bone. Furthermore, tantalum could stimulate cell proliferation, and improve the ability of osteogenesis of human osteoblasts.[17] Different types of tantalum interbody fusion implants evolved over time in shape and quality. A new generation of porous tantalum called trabecular metal (TM) came into being, with good biocompatibility, high porosity and bone similar elastic modulus characteristics. Clinically, TMs (such as porous tantalum) are widely used in avascular necrosis of the femoral head, artificial joints, spinal fusion, and other fields.[18-25] Especially in the treatment of early avascular necrosis of the femoral head and total hip/knee reconstruction in situations of massive bone defect, remarkable results could be achieved compared with the traditional materials and methods of treatment.[19-22,24] Recently, several clinical studies have been undertaken on the use of porous tantalum for spinal interbody fusion.[18,25-29] TM has been proved effective in obtaining fusion and improving clinical outcome in patients after lumbar interbody fusion (LIF).[26-29] However, different fusion rates have been reported in anterior cervical interbody fusion by TM implants. Löfgren et al[30] reported that TM showed a lower fusion rate (69%) than autograft group (92%) after single-level anterior cervical fusion which led to controversial views among spine surgeons. Zardiackas et al[31] evaluated a porous tantalum biomaterial (Hedrocel) and the results demonstrated a significant variation in the single-cycle mechanical properties of the porous tantalum, which was probably caused by the differences in morphology and processing that resulted in less precisely controlled microstructural parameters. Shimko et al[32] explored the effect of porosity on the

fluid flow characteristics and mechanical properties of TM, and they concluded that a better understanding of these structure-function relationships was benefit for enhancing quality of the implant designs.

A biomedical porous tantalum synthesized via three-dimensional knitted wire framework and chemical vapor deposition (CVD), was applied to *in vitro* and *in vivo* experiments. The purposes of the present study were to evaluate the biocompatibility and osteocompatibility of the novel porous tantalum implant, and to evaluate the efficacy to achieve LIF by assessing the radiographic and histologic performance between the novel porous tantalum implant and autologous bone in a rabbit anterior lumbar fusion model.

Methods

Ethical approval

The study was approved by the Animal Care and Use Committee of The Third Affiliated Hospital of Southern Medical University, according to the National Institute of Health Guide.

Experimental animals and design

A total of 24 adult healthy New Zealand rabbits (12 males and 12 females), aged 2–3 months and weight 2.0–2.3 kg (average 2.2 kg), were maintained under the same housing conditions. Each rabbit underwent an anterior discectomy with or without intervertebral lumbar arthrodesis at 3 levels: L3–L4, L4–L5, and L5–L6. Each level was randomly allocated to be performed one of the 3 procedures: (1) discectomy only (control group); (2) discectomy with autologous bone implanted (autograft group); and (3) discectomy with porous tantalum implanted (tantalum group). All the 24 rabbits were randomly sacrificed at the different times: 2 months ($n = 6$), 4 months ($n = 6$), 6 months ($n = 6$), and 12 months ($n = 6$).

Porous tantalum spine implants

A cubic porous tantalum (Ning Xia Orient Tantalum Industry Co. Ltd, Shizuishan, China) synthesized via 3-dimensional knitted wire framework and CVD (length, width, and height of 2.5–3.0 mm; Figure 1A) was used in this study. The porosity was determined by the porous tantalum volumes and their net weights. It was calculated by the equation: porosity (%) = $(1 - M_{porous}/M_{Ta}) \times$ 100%. Here, M_{porous} was the weight of the porous block (measured) while M_{Ta} represented the weight of pure and solid Ta block with the same volume of the corresponding porous one. The morphology of porous tantalum block was further characterized through a Zeiss Ultra Plus field emission scanning electron microscopy (FESEM; Zeiss, Stuttgart, Germany). The FESEM was equipped with an energy dispersive spectral (EDS) X-ray detector (Shimadzu, Tokyo, Japan), which could be applied for the element determination through the particle-induced X-ray spectra (PIXS; Shimadzu). An operation voltage of 10 kV was set for the FESEM, which would be enough to excite the M and L electrons of Ta atoms.
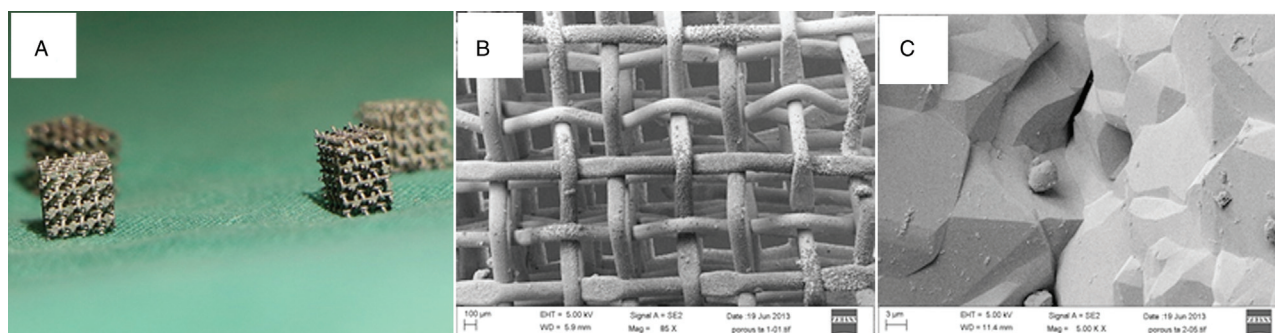
Figure 1: The novel porous tantalum implants. (A) The outlook of cubic porous tantalum implants (length, width and height were 2.5–3.0 mm). The scanning electron microscopic images of porous tantalum in a lower magnification (B; ×85) and a higher magnification (C; ×5000).

Surgical procedure

All rabbits were fasted for 24 hours prior to surgery. Anesthesia was maintained with injection of 2% sodium pentobarbital (30 mg/kg; Sigma, MO, USA). For autologous grafting, an approximately 30 mm³ tricortical iliac crest autograft was harvested using an osteotome and mallet, and further cut into cubes so that it could be implanted into the intervertebral space. For discectomy and spinal fusion surgery, the rabbit was put into supine position with the abdomen prepared and draped. A paramedian abdominal incision was conducted and a transperitoneal anterior approach was used. The L3–L4, L4–L5, and L5–L6 intervertebral discs and the superior and inferior endplates were excised together with part of the anterior longitudinal ligament. Then each level was randomly allocated to be performed one of the 3 procedures: (1) discectomy only; (2) discectomy with autologous bone implanted; and (3) discectomy with tantalum implanted. The wound was carefully sutured after being washed and hemostasis. Penicillin (40,000 U/kg, Sigma) was given before and immediately after surgery, and twice a day for 3 consecutive days to prevent infection.

General observation and neurologic evaluations

Wound healing conditions and hind leg movements were closely observed after surgery. Neurologic evaluations were conducted at 1 week post-operative and before euthanasia (2, 4, 6, and 12 months post-operative). The neurologic evaluation criteria were as follows[33]: 0, walking without any detectable ataxia; 1, walking, slightly ataxic; 2, walking, but with noticeable weakness on one side or both sides; 3, able to stand on forelimbs but dragging rear limbs; and 4, recumbent and unable to rise.

Radiographic and micro-computed tomography evaluation

Radiographs of lumbar spine (anteroposterior and lateral views) were taken immediately after surgery to determine the position of tantalum implants and bone grafts. At 2, 4, 6, and 12 months post-operatively, 6 rabbits were randomly selected to sacrifice and obtain the lumbar specimens, respectively, which were set for micro-computed tomography (micro-CT) examination (SCANCO, Zurich, Switzerland). The spinal fusion performance of the operation segments was reviewed on sagittal plane micro-CT views by 3 evaluators in a double-blind condition. Brantigan-Steffee classification was applied to confirm the existence of fusion.[34] The criteria included: the bone in fusion area is denser and more mature than originally achieved during surgery, no interspace between the implant (tantalum or autograft) and the vertebral body, and mature bony trabeculae bridging in fusion area. Any one of the above 3 criteria not reached would be defined as non-fusion state. The fusion index scoring according to the Bridwell grading system was as following[35]: 0, fusion absent with collapse/resorption of the graft; 1, graft intact, potential lucency present at the top and bottom of the graft; 2, graft intact, not fully remodeled and incorporated, but no lucency present, implies partial fusion (meet 1 or 2 criteria of Brantigan-Steffee classification); and 3, fused with remodeling and trabeculae present, impling complete fusion (meet all 3 criteria of Brantigan-Steffee classification). At each time point, the number of specimens meeting the criteria of complete fusion was recorded. The fusion rate was calculated by the equation: fusion rate (%) = N_f/$N_t \times 100\%$. Here, N_f was the number of complete fusion specimens and N_t was the total number of specimens observed.

Histologic examination

Histologic examination was performed in specimens at 12 months post-operatively. Lumbar spine specimens were trimmed and fixed in 4% paraformaldehyde for 12 hours, dehydrated with graded alcohols and then embedded in methylmethacrylate without decalcification. Longitudinal cutting of 20 μm thick hard tissue sections were performed using a LEICA SP1600 microtome (LEICA, Heidelberg, Germany). Only slices near the central sagittal plane were used for subsequent experiments. Histochemical staining for toluidine blue was done according to the manufacturer's instruction on these sections of bone, and microscopic examinations were performed using a Nikon ECLIPSE E600 stereomicroscope outfitted with a Nikon Digital Camera DXM1200. The histologic slides and microscopic images were used to evaluate the presence of histologic fusion or pseudarthroses. The criterion used to assess histologic fusion was the existence of a continuous bony bridge from the cranial to the caudal vertebra. Analysis of the stained undecalcified sections was also used to determine the histologic and cytologic response to the

treatments and osteocompatibility of the porous tantalum plant.

Bone marrow-derived mesenchymal stem cell culture on porous tantalum plant

Bone marrow cells were isolated by flushing the bone marrow spaces of femora and tibiae of 1 New Zealand rabbit. Bone marrow cell suspension was prepared by flushing the diaphysis with F-12K and 10% fetal bovine serum for 3–5 times. Bone marrow cells were plated in 75 cm^2 tissue flasks in 10 mL of bone marrow-derived mesenchymal stem cells (BMSCs) media at 37°C with 5% CO_2. After 72 hours, the supernatant and non-adherent cells were removed and fresh medium was added. When BMSCs achieved 85% confluence, adherent cells were trypsinized and collected for further assays. All media were supplemented with 2 mmol/L glutamine, 100 U/mL penicillin, and 100 μg/mL streptomycin. Cells at the third passaged generation were used for culture on the sterilized porous tantalum plant.

The BMSCs were seeded on porous tantalum plant in a 96-well plate with a cell density of 3×10^4 cells/mL, and cultured for another 7 days in complete α-medium. The cell culture media was replaced every other day. To observe cell morphology, the cells on the porous tantalum plant were fixed with 4% glutaraldehyde solution for 3 hours, washed with phosphate-buffered saline solution, and again fixed in 2% osmic acid, and dried for 1 hour. Then the constructs were dehydrated using a graded ethanol series and then transferred to isoamyl acetate, dried at CO_2 critical point, and observed under scanning electron microscope (SEM, H-3000N; HITACHI, Tokyo, Japan).

Cell counting kit-8 assay

Cell counting kit-8 (CCK-8; Dojindo, Tokyo, Japan) provides a tool for determining the toxicity in cell proliferation by utilizing highly water-soluble tetrazolium salt. Sterilized porous tantalum plant was immersed in the medium for 48 hours and the leaching liquor medium was collected. Then BMSCs were treated with 200 μL leaching liquor culture medium for 5 days in a 96-well plate (leaching liquor group). The control group was treated with 200 μL culture medium without leaching liquor for 5 days and then 20 μL of CCK-8 solution was added to each well for an additional 4 hours. The absorbance was measured at 450 nm on an automated microtiter plate reader. Data were expressed as the mean percentage of viable cell vs. control.

Statistical analysis

All data are presented as the mean± standard deviation. Comparison of fusion index scores was analyzed between groups using one-way analysis of variance. Other comparisons of numerical variables between groups were made by Student t test. All statistical analyses were performed using SPSS version 19.0 (IBM Corp., Armonk, NY). A $P < 0.05$ was considered statistically significant.

Results

Porous tantalum implants

The outlook and SEM of the porous tantalum are depicted in Figure 1. From the SEM image, it could be seen that the porous tantalum had a completely open construction, which was beneficial to the bone ingrowth into the implant interface, so as to achieve the goal of stable fusion. It was tested by SEM that the pore size was about 500 μm in a cubic shape, and the pores in porous tantalum were totally connected, with an average porosity of 86.8% [Figure 1B]. Such a porosity was much higher than these reported in previous literatures.[36,37] The connection of porous tantalum frame was similar to diamond crystal lattices, which could ensure very strong physical strength between different layers. A zoomed SEM image showed that the joints between different wires were connected by the deposited tantalum reduced from CVD [Figure 1C]. Indeed, the present joining procedure has reinforced the structure stability, as well as the hardness of the sample. It was also interesting to note here that the wire surface was rather rough. A roughness up to tens of micrometers could be found. Such a rough surface would further help the bone grown/deposited on the surface of the frame. The Young module of the porous tantalum was calculated to 0.6 GPa, which was similar but slightly higher than the human's bones. In addition, it was important to note that the porosity could be adjusted through different knitting structures of the tantalum frames. This increased the availability to tailor the present material into different implanting positions.

A spot was further selected for the EDS analysis to determine the element components. The selected spot and the PIXS are shown in Figure 2. The spot size was about 50 μm in diameter [Figure 2A]. Bombarded by the 10 keV electrons in FESEM, the present samples emitted characteristic X-rays which would be further recorded by the detector. The PIXS showed that all the emitted X-ray photons were the characteristic transitions after the decaying of L- and M-holes of tantalum [Figure 2B]. No other elements, such as chlorine as the raw material or carbon, were detected. The EDS proved that the porous tantalum produced through the present route was pure without ambient or intermediate contaminations.

Experimental rabbits

All rabbits survived and recovered walking activities gradually after operation, without any symptoms of nerve injury. Neurologic function scores of all experimental rabbits were 0 (normal, no symptoms of nerve injury, walking without, any detectable ataxia) at 1 week post-operative and before euthanasia (2, 4, 6, and 12 months post-operatively, respectively). One case had incision infection and healed after symptomatic treatment. Abdominal wall hernia occurred in 1 case.

Radiographic results

A post-operative radiograph showed the non-radiolucent tantalum implant was implanted into the intervertebral space, while the autograft implantation and discectomy
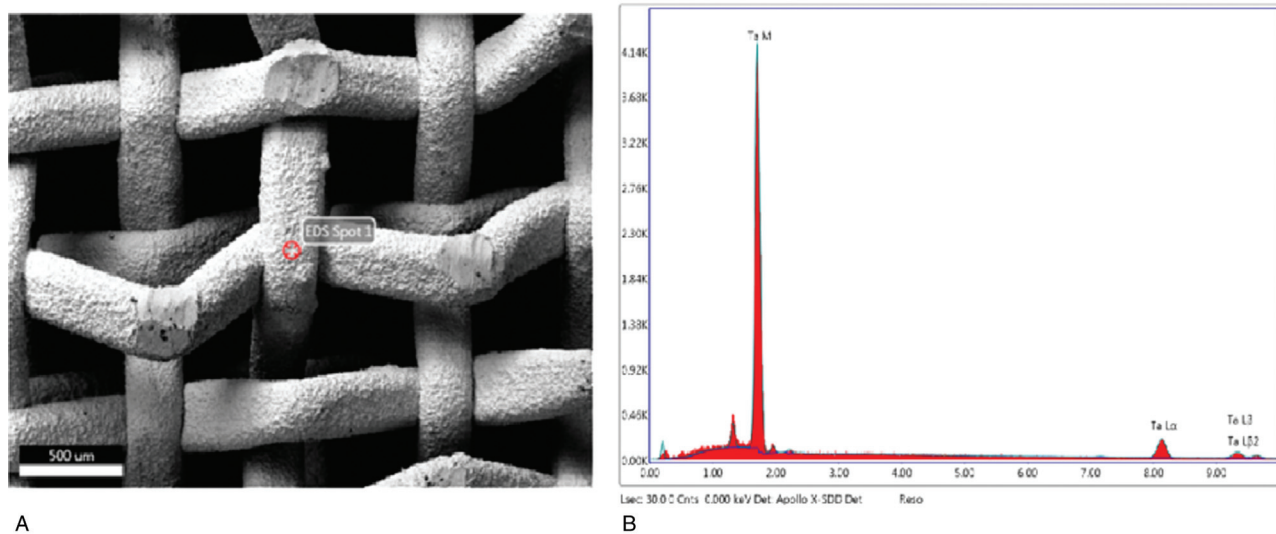
Figure 2: The energy dispersive spectral analysis to determine the element components of the porous tantalum implant. (A) Spot (red circle) selected for the energy dispersive spectral determination. (B) Energy dispersive X-ray spectrum measured from porous tantalum. No other elements, such as chlorine as the raw material or carbon, were detected.
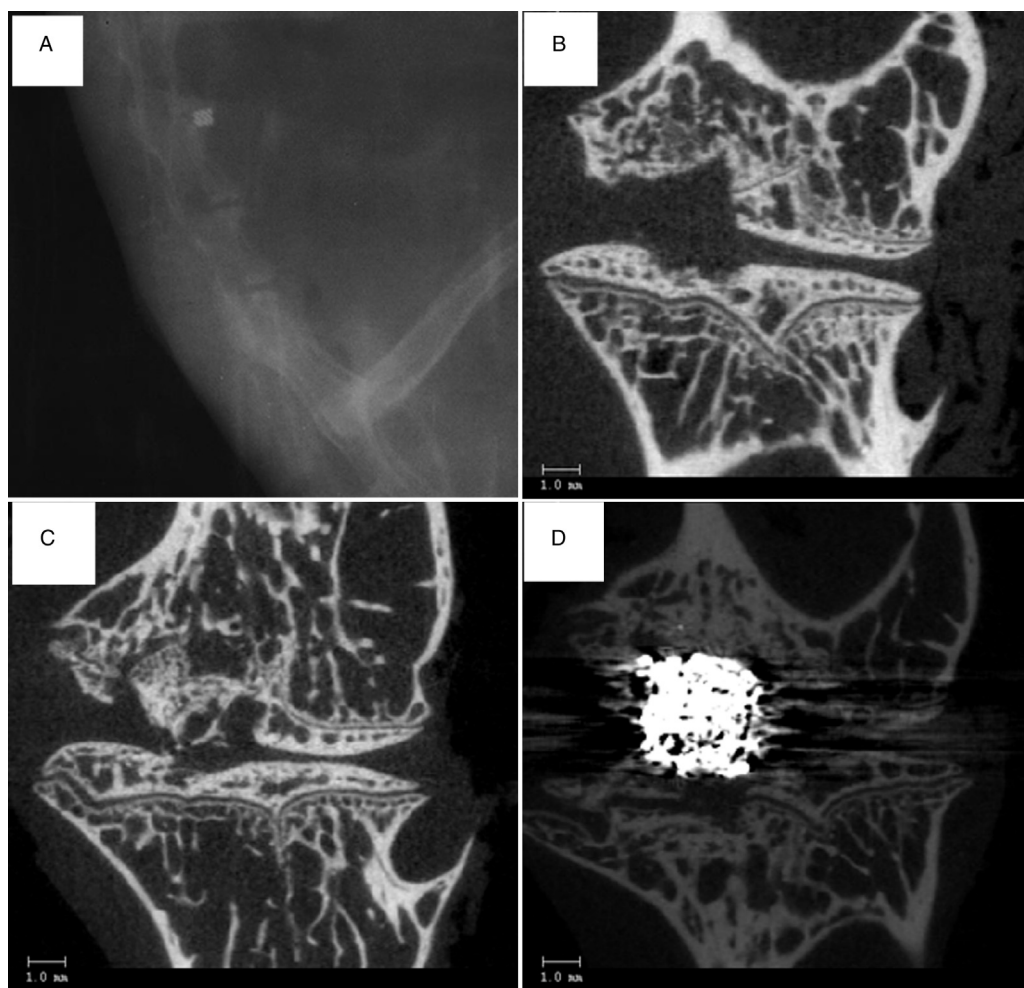
Figure 3: Imaging of operative lumbar spine segments of the New Zealand rabbits. (A) Post-operative lateral radiograph showing a non-radiolucent tantalum implant was implanted into the L3–L4 intervertebral space. (B) Micro-computed tomography (micro-CT) image of discectomy only space (control group) showing the appearance of the defect after discectomy in the intervertebral space. (C) Micro-CT image showing discectomy with autologous bone implanted space (autograft group). (D) Micro-CT image showing discectomy with porous tantalum implanted space (tantalum group).

only spaces were both radiolucent [Figure 3A]. CT scan confirmed that the tantalum implant and autologous bone were located in the anterior portion of the intervertebral space [Figure 3C and 3D], while discectomy only space showed the appearance of the defect after operation [Figure 3B].

Figure 4 showed micro-CT scan images of the spinal fusion performance achieved upon implantation of tantalum implants in different periods post-operative. A few artifacts could be seen around the tantalum implants on the micro-CT scan images. However, it did not affect the decision making of measurement of fusion success. It was found that there was a clear radiolucent zone around the tantalum implant at 2 months after the operation, implying non-fusion state [Figure 4A]. Obvious new bone formation and trabecular structure were observed around the tantalum implant at 4 months after operation, which implied partial fusion state [Figure 4B]. At 6 months post-operatively, obviously remodeling with trabeculae across intervertebral space and existence of bony bridging around the tantalum implant were observed, which implied probably fusion [Figure 4C]. While at 12 months post-operatively, completely remodeling with trabeculae across intervertebral space and enwrapping the tantalum implant

with overgrowth of bridging bone beyond the vertebral anterior edge were observed as the most important parameters for measurement of complete fusion success [Figure 4D].

Figure 5 showed sagittal plane micro-CT views of intervertebral spaces in the 3 different procedures at 12 months post-operatively. Both autograft and tantalum implanted spaces showed solid fusion with continuous bony bridge from the cranial to the caudal vertebra [Figure 5B and 5C], while lucency present at intervertebral space was observed in discectomy only segment [Figure 5A], which implied non-fusion.

Mean fusion index scores of the control group, autograft group, and tantalum group at different sacrifice times are shown in Table 1. Control group had a mean fusion index score of 0 at all different sacrifice times, indicating that no spontaneous fusion of the intervertebral spaces was observed after discectomy. Both in tantalum and autograft groups, the fusion index scores of 6 and 12 months tended to be higher than the scores of 2 and 4 months ($F = 122.83$, $P < 0.001$ for tantalum group; $F = 52.71$, $P < 0.001$ for autograft group). Nevertheless, the difference between 6 and 12 months was statistically significant in autograft group ($F = 52.71$, $P =$
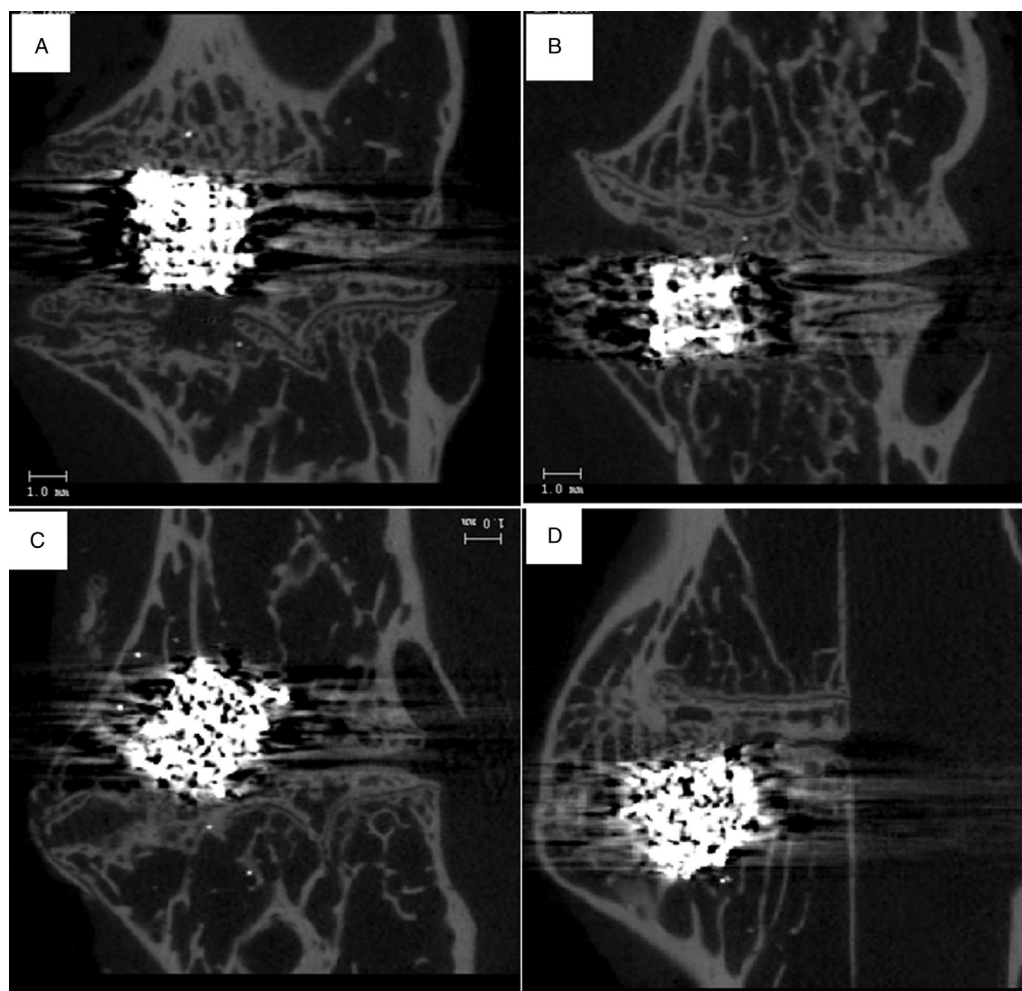
Figure 4: Micro-computed tomography images of the spinal fusion performance achieved upon implantation of tantalum implants in different post-operative periods: (A) 2 months post-operatively; (B) 4 months post-operatively; (C) 6 months post-operatively; and (D) 12 months post-operatively.
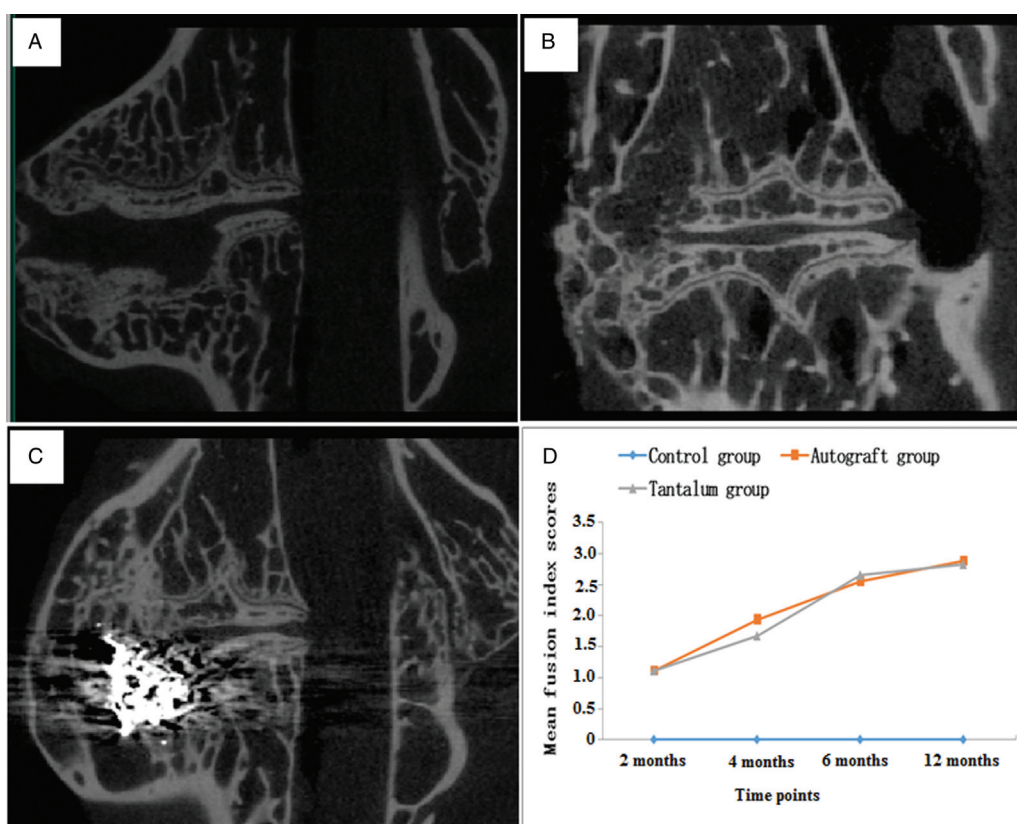
Figure 5: Micro-computed tomography images of operative lumbar intervertebral spaces in the 3 different procedures at 12 months post-operatively: (A) discectomy only space (control group); (B) discectomy with autologous bone implanted space (autograft group); and (C) discectomy with porous tantalum implanted space (tantalum group). Both autograft and tantalum groups developed solid fusion with continuous bony bridge from the cranial to the caudal vertebra, while non-fusion was observed in control group. (D) The imaging fusion index scores at different post-operative time points.

0.009), but was not significant in tantalum group ($F = 122.83$, $P = 0.195$). Radiographic fusion index scores at 12 months post-operatively between autograft and tantalum groups showed no significant difference (2.89 ± 0.32 vs. 2.83 ± 0.38, $F = 244.60$, $P = 0.709$).

Histologic results

Representative images of the stained undecalcified sections at 12 months post-operatively are illustrated in Figure 6. Histologic results showed trabecular bone ingrowth into the porous tantalum implant from all directions with junction fusion at implant interface [Figure 6C]. In autograft specimen section, a continuous bony bridge

with cartilage formation and endochondral ossification from the cranial to the caudal vertebra was observed [Figure 6B]. While in discectomy only specimen, a gap with fibrous tissue surrounding at the intervertebral space was observed, which indicated non-fusion [Figure 6A].

Micro-CT evaluation and histologic examination for fusion were highly correlated in this study. Both in the tantalum and autograft groups (12 months post-operatively), the histologic fusion rate was 100.0% (6/6). No fusion was observed in the control group (0/6).

Both the autograft and porous tantalum stained undecalcified sections showed fragments of necrotic bone surrounding by histologic viable bone [Figure 7]. New bone formation was associated with osteonecrosis which illustrated the process of bone remodeling and fusion. The tantalum device interface consisted of direct bone contact, and no implant degradation, wear debris, or osteolysis was observed. No significant local inflammation response was found around or in the tantalum implant materials [Figure 7B].
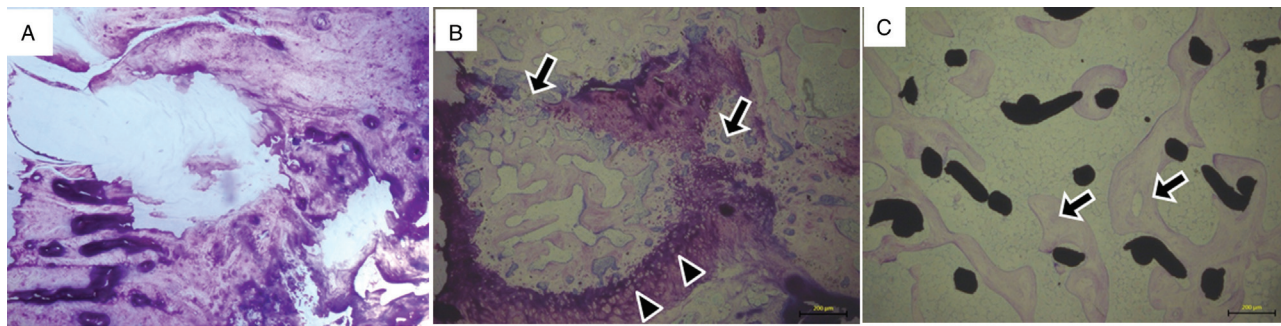
Cell toxicity and biocompatibility results

The CCK-8 assay showed no significant difference of absorbance values between the leaching liquor group and control group (1.25 ± 0.06 vs. 1.23 ± 0.04, $t = -0.644$, $P = 0.545$), which indicated the BMSC proliferation without toxicity. BMSC attachment and proliferation in the porous

Table 1: Radiographic fusion index scores for 3 different procedures at different sacrifice times

Post-operative times	Control group	Autograft group	Tantalum group
2 months ($n = 6$)	0	1.11 ± 0.68	1.11 ± 0.32
4 months ($n = 6$)	0	1.94 ± 0.80	1.67 ± 0.49
6 months ($n = 6$)	0	$2.56 \pm 0.70^{*,\dagger}$	$2.66 \pm 0.49^{*,\dagger}$
12 months ($n = 6$)	0	$2.89 \pm 0.32^{*,\dagger,\ddagger}$	$2.83 \pm 0.38^{*,\dagger}$

Data are shown as mean ± standard deviation. $^{*}P < 0.05$, vs. the score of 2 months in the same group; $^{\dagger}P < 0.05$, vs. the score of 4 months in the same group; $^{\ddagger}P < 0.05$, vs. the score of 6 months in the same group.

Figure 6: Representative images of the stained undecalcified sections at 12 months post-operatively. (A) Control group: a clapse gap with fibrous tissue surrounding at the intervertebral space was observed (hematoxylin and eosin staining, ×50). (B) Autograft group: histologic fusion is demonstrated by continuous cranial to the caudal bony bridging with cartilage formation (triangle) and endochondral ossification (arrows) in the intervertebral space (hematoxylin and eosin staining, ×50). (C) Tantalum group: histologic fusion is demonstrated by continuous cranial to the caudal bony bridging with newly formed bone trabecular (arrows) ingrowth into the porous tantalum (hematoxylin and eosin staining, ×50).
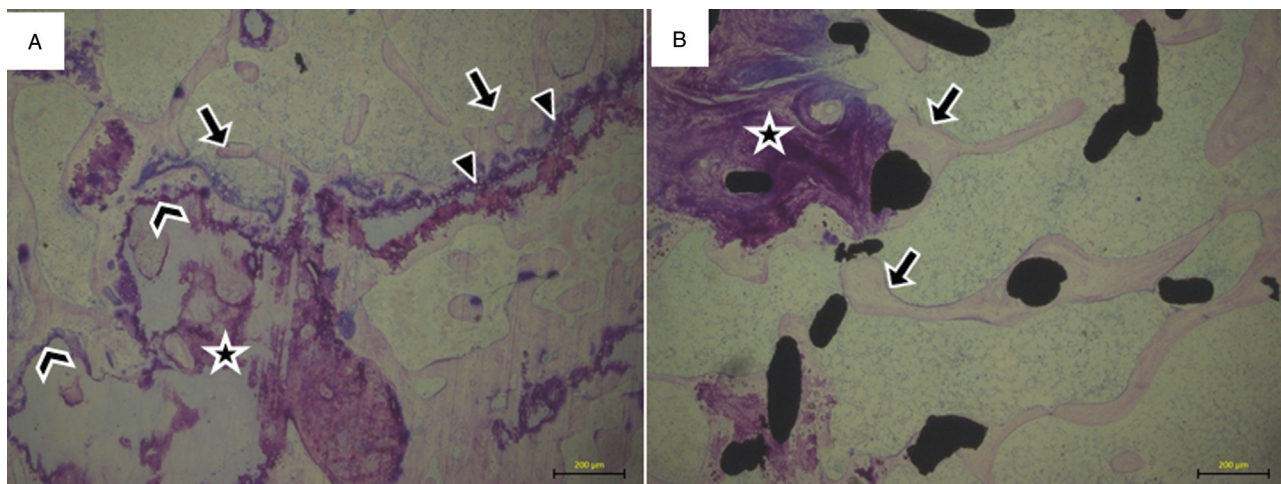
Figure 7: Stained undecalcified sections showing new bone formation associated with osteonecrosis in (A) autograft and (B) porous tantalum interface (hematoxylin and eosin staining, ×50). Cartilage formation (triangles) and endochondral ossification (arrows) associated with necrotic bone (pentagrams) and cement lines (dovetails) representing the process of bone remodeling. No implant degradation, bone resorption or significant local inflammation response was observed in tissue adjacent to the tantalum implant.

tantalum plant were observed after 7 days culture. The morphology of the BMSCs cultured on the tantalum plant was examined by SEM [Figure 8]. At lower magnification, the cells were found formed a continuous layer on the surface of tantalum and grew into the pores [Figure 8A]. At higher magnification, these cells showed irregular shapes with long spindles adhered to the surface of tantalum implant [Figure 8B]. These results indicated that the composites and degradation products of the tantalum implant were non-toxic and with good biocompatibility.

Discussion

This study evaluated the cell toxicity and biocompatibility of tantalum implant in BMSC culture *in vitro*. The results showed that the tantalum implants were non-toxic and with good biocompatibility. Furthermore, this study evaluated the bone tissue ingrowth into the tantalum implants in different times after intervertebral fusion surgery by micro-CT and histologic studies. All 6 rabbits treated with tantalum implants achieved histologic fusion at 12 months post-operatively. The tantalum implants

were completely fused with the surrounding bone tissue. Similar results were achieved with autologous bone grafts, which confirmed that the novel porous tantalum could be used as an effective bone substitute for spinal fusion. For control group, it was clearly able to make a determination of non-fusion state in histologic sections by observation of a clapse gap with fibrous tissue surrounding at the intervertebral space. These were further confirmed by micro-CT evaluators that discectomy only levels had a mean fusion index score of 0 at all different sacrifice times, excluding the possibility of spontaneous fusion of the discectomy intervertebral space. While in autograft and tantalum groups, the mean fusion index scores were 2.56 ± 0.70 and 2.66 ± 0.49 at 6 months (indicating partial fusion) and 2.89 ± 0.32 and 2.83 ± 0.38 at 12 months (close to complete fusion), respectively. Bony radiologic changes progress was observed from the micro-CT images that the intervertebral bone fusion extended from the inside and around the tantalum plant to the vertebral anterior cortical edge, and overgrowth of bridging bone beyond the vertebral anterior edge was observed finally. Nevertheless, the extent of bone fusion was observed only invertebral anterior edge, which might due to that the
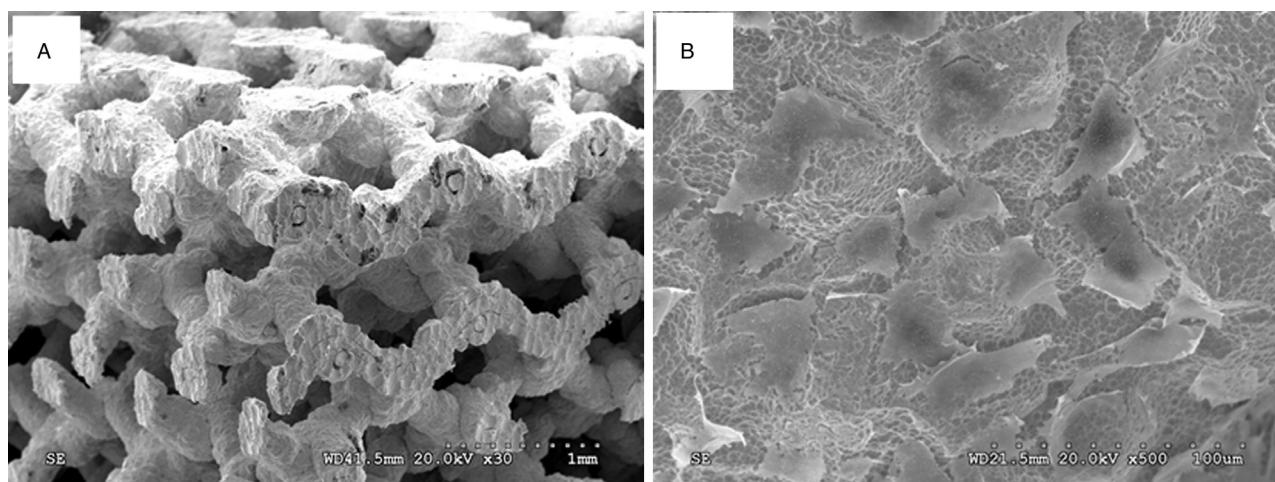
Figure 8: Morphology of bone marrow-derived mesenchymal stem cells cultured on tantalum implant. (A) The images of scanning electron microscope showing that the cells formed a continuous layer on the surface of tantalum and grew into the pores at lower magnification (×30). (B) The cells showed irregular shapes with long spindles adhered to the surface of tantalum implant at higher magnification (×500).

posterior portion of the intervertebral disc was reserved to avoid nerve damage during operation.

The LIF is widely used as a surgical treatment procedure for chronic degenerative spondylosis. Various types of intervertebral cages have become prevalent for maintaining the stability of fusion segment and preventing the disc space from collapsing during the healing process.[38-43] The titanium cage has been reported to be effective with a fusion rate of 90% in single-level LIF, and 70–80% in patients with multi-level LIF.[39-41] However, it is difficult to determine of fusion in radiographic examination due to the considerable metallic artifact around the cage. Potential errors in identifying the quality of fusion were from metallic artifact. Underestimate lucencies tended to be observed in metallic implants.[44,45] Then, a radiolucent spine fusion cage made by polyether ether ketone (PEEK) packed with autograft is widely used in the treatment of spine degenerative disc disorders with good clinical results.[46] Kim et al[47] described a typical bony radiologic change progress to the cortical margin in intervertebral space in a long time follow-up clinical study. Nevertheless, complications such as migration and subsidence of the cage consequent to non-fusion were observed frequently,[48-50] which might due to a lack of osteogeneration and fibrous tissues enwrapping the PEEK cages.[33] Porous tantalum cages show better biocompatible and osteoconductive properties, especially the high porosity and bone similar structure allowing trabecular bone ingrowth into the porous tantalum cages, thus achieving a better osteointegration encapsulating the cage. Besides, it shows an increased radiolucency and decreased artifact than titanium cage. Therefore it is expected that the porous tantalum could be a better biomaterial for interbody fusion cages due to the increased fusion rate and radiolucency.

The successful clinical fusion of a spinal implant depends on various biologic and clinical factors, as well as on the properties of implant materials. Surface or structural parameters modification of orthopedic implants also has been shown to enhance osteoconductive property.[17,51-53]

Zou et al[54] and Huang et al[55] reported an experimental study about bone ingrowth in porous tantalum implants (Zimmer Inc., Colorado, USA) on spinal fusion in pigs. New trabecular bone ingrowth through the central hole of porous tantalum ring and grow into porous tantalum implant were observed in histologic study. Their results were similar to the findings of this study, except that this study used a cubic tantalum metal implant based on the 3-dimensional knitted wire framework and CVD, which could provide a high degree of porosity in structure, conducive to bone tissue ingrowth on the interface between bone and implant, so as to achieve the purpose of solid fusion. The advantages of this novel synthesizing route of forming porous tantalum were that the pore size, porosity, compressive strength, and the Young modulus could be easily modified by the thicknesses of tantalum film and the structure of knitted framework. Besides, it could produce porous tantalum implants with precisely controlled 3-dimensional microstructural and effectively desired mechanical properties, which could show more stable and controllable stiffness, providing sufficient compressive strength and comparable stiffness during the process of spine interbody fusion.

Radiologic imaging such as CT and X-ray were usually used as a realistic and efficient method to confirm the existence of a fusion segment. The Brantigan-Steffee classification is widely used to confirm successful intervertebral fusion.[34] The criteria include: the bone in fusion area is more dense and more mature than originally achieved during surgery, no interspace between the cage and the vertebral body, and mature bony trabeculae bridging in fusion area. Kim et al[56] emphasized a new parameter that no traction spur formation should be added to the fusion criteria after a posterior lumbar interbody fusion (PLIF) procedure. McAfee[57] emphasized that the formation of bony trabeculae bridging was the most important parameter for evaluation of fusion success. Similarly, the results of this study showed that both autograft and tantalum implanted spaces with a visible continuous bony bridge from the cranial to the caudal vertebra at 12 months post-operatively.

Microscopic images of specimens at 12 months post-operatively stained with toluidine blue showed new bone formed and filled the intervertebral space or porous tantalum implant, and connected the cranial and the caudal vertebra bodies. While in discectomy only specimen, fibrous tissue surrounding at the intervertebral space without new bone formation was observed. The results suggested that characteristics of the fusion induced by porous tantalum implant were similar to those of autograft bone. The adjacent vertebral bodies did not induce spontaneous fusion after discectomy without interface contact. Togawa et al[58] obtained tissue from radiographically successful human intervertebral body fusion cages by needle biopsies, and they found that autogenous bone graft was incorporated with small fragments of necrotic bone associated with histologic viable bone. Similarly, this study found cartilage formation and endochondral ossification were associated with osteo-necrosis and cement lines representing the process of bone remodeling. Particles of debris could originate from the implant cages degradation products or friction debris. Previous studies have reported the osteolysis caused by wear debris, due to the excessive inflammatory reaction con-ducted by macrophages.[59-61] Osteolysis represents a step-wise histolytic response to wear debris. Thus, it is an important indicator to evaluate the quality of implants for bone remodeling and fusion. In the present study, there was no implant degradation, bone resorption or significant local inflammation response, probably reflecting very few or no particles of debris emerged during the bone fusion.

The limitation in the current study was that we did not perform biomechanical testing, because any biomechanical testing might cause damage of the fibrous tissue and bony bridging formed inside and around the implants. We wanted to keep intact interface between the host bone and the autograft or tantalum implant in the stained undecalcified sections. Further investigations on examin-ing full-thickness load-bearing repairs in bone should be conducted to better understand this new porous tantalum's full structure-function relationships and clinical potential.

In conclusion, this study evaluated the osteocompatibility and the efficacy to achieve LIF of the novel porous tantalum implant in vitro and in vivo. Radiographic and histologic fusion was observed in the porous tantalum as similar as in autologous bone implanted intervertebral spaces in a rabbit anterior lumbar fusion model at 12 months post-operatively. No implant degradation, wear debris, or osteolysis was observed. No significant local inflammation response was found around or in the tantalum implant materials. The composites and degrada-tion products of the tantalum implant were non-toxic and with good biocompatibility. According to these results, it was expected that the novel porous tantalum could be a valid biomaterial for interbody fusion cages.

Conflicts of interest

None.

Author contributions

Lu M: conception and design, collection and assembly of the data, data analysis and interpretation and manuscript writing; Xu S: collection and assembly of the data, data analysis and interpretation; Lei ZX: collection and assembly of the data; Lu D: design of the novel porous tantalum implant; Cao W, Huttula M, Hou CH, Du SH and Chen W: collection and assembly of the data; Li HM: providing advice on experimental design and data analysis; Jin DD: design and supervision of the study. All authors reviewed and commented on the manuscript.

References

1. Ghogawala Z, Whitmore RG, Watters WC 3rd, Sharan A, Mummaneni PV, Dailey AT, et al. Guideline update for the performance of fusion procedures for degenerative disease of the lumbar spine. Part 3: assessment of economic outcome. J Neurosurg Spine 2014; 21:14–22. doi: 10.3171/2014.4.SPINE14259.
2. Ransom BR, Neale E, Henkart M, Bullock PN, Nelson PG. Mouse spinal cord in cell culture. I. Morphology and intrinsic neuronal electrophysiologic properties. J Neurophysiol 1977; 40:1132–1150. doi:10.1152/jn.1977.40.5.1132.
3. Li JJ, Gil ES, Hayden RS, Li C, Roohani-Esfahani SI, Kaplan DL, et al. Multiple silk coatings on biphasic calcium phosphate scaffolds: effect on physical and mechanical properties and in vitro osteogenic response of human mesenchymal stem cells. Biomacromolecules 2013; 14:2179–2188. doi: 10.1021/bm400303w.
4. Lou T, Wang X, Song G, Gu Z, Yang Z. Fabrication of PLLA/(-TCP nanocomposite scaffolds with hierarchical porosity for bone tissue engineering. Int J Biol Macromol 2014; 69:464–470. doi: 10.1016/j.ijbiomac.2014.06.004.
5. Moreau MF, Gallois Y, Baslé MF, Chappard D. Gamma irradiation of human bone allografts alters medullary lipids and releases toxic compounds for osteoblast-like cells. Biomaterials 2000; 21:369–376. doi:10.1016/S0142-9612(99)00193-3.
6. Moreland DB, Asch HL, Clabeaux DE, Castiglia GJ, Czajka GA, Lewis PJ, et al. Anterior cervical discectomy and fusion with implantable titanium cage: initial impressions, patient outcomes and comparison to fusion with allograft. Spine J 2004; 4:184–191. doi:10.1016/j.spinee.2003.05.001.
7. Peolsson A, Vavruch L, Hedlund R. Long-term randomised comparison between a carbon fibre cage and the Cloward procedure in the cervical spine. Eur Spine J 2007; 16:173–178. doi:10.1007/s00586-006-0067-2.
8. Wigfield CC, Nelson RJ. Nonautologousinterbody fusion materials in cervical spine surgery: how strong is the evidence to justify their use? Spine 2001; 26:687–694. doi:10.1097/00007632-200103150-00027.
9. Banwart JC, Asher MA, Hassanein RS. Iliac crest bone graft harvest donor site morbidity. A statistical evaluation. Spine 1995; 20:1055–1060. doi:10.1097/00007632-199505000-00012.
10. Dimitriou R, Mataliotakis GI, Angoules AG, Kanakaris NK, Giannoudis PV. Complications following autologous bone graft harvesting from the iliac crest and using the RIA: a systematic review. Injury 2011; 42 (Suppl. 2):S3–S15. doi: 10.1016/j.injury.2011.06.015.
11. Schnee CL, Freese A, Weil RJ, Marcotte PJ. Analysis of harvest morbidity and radiographic outcome using autograft for anterior cervical fusion. Spine 1997; 22:2222–2227. doi:10.1097/00007632-199710010-00005.
12. Silber JS, Anderson DG, Daffner SD, Brislin BT, Leland JM, Hilibrand AS, et al. Donor site morbidity after anterior iliac crest bone harvest for

single-level anterior cervical discectomy and fusion. Spine 2003; 28:134–139. doi:10.1097/00007632-200301150-00008.

13. Hou CH, Yang RS, Hou SM. Hospital-based allogenic bone bank–10-year experience. J Hosp Infect 2005; 59:41–45. doi:10.1016/j.jhin.2004.03.017.

14. Kretlow JD, Mikos AG. Review: mineralization of synthetic polymer scaffolds for bone tissue engineering. Tissue Eng 2007; 13:927–938. doi:10.1089/ten.2006.0394.

15. Stewart M, Welter JF, Goldberg VM. Effect of hydroxyapatite/tricalcium-phosphate coating on osseointegration of plasma-sprayed titanium alloy implants. J Biomed Mater Res A 2004; 69:1–10. doi:10.1002/jbm.a.20071.

16. Yang W, Both SK, van Osch GJ, Wang Y, Jansen JA, Yang F. Performance of different three-dimensional scaffolds for in vivo endochondral bone generation. Eur Cell Mater 2014; 27:350–364. doi:10.3233/BIR-140658.

17. Sagomonyants KB, Hakim-Zargar M, Jhaveri A, Aronow MS, Gronowicz G. Porous tantalum stimulates the proliferation and osteogenesis of osteoblasts from elderly female patients. J Orthop Res 2011; 29:609–616. doi: 10.1002/jor.21251.

18. Fernández-Fairen M, Sala P, Dufoo M Jr, Ballester J, Murcia A, Merzthal L. Anterior cervical fusion with tantalum implant: a prospective randomized controlled study. Spine 2008; 33:465–472. doi: 10.1097/BRS.0b013e3181657f49.

19. Long WJ, Scuderi GR. Porous tantalum cones for large metaphysealtibial defects in revision total knee arthroplasty: a minimum 2-year follow-up. J Arthroplasty 2009; 24:1086–1092. doi: 10.1016/j.arth.2008.08.011.

20. Meneghini RM, Lewallen DG, Hanssen AD. Use of porous tantalum metaphyseal cones for severe tibial bone loss during revision total knee replacement. Surgical technique. J Bone Joint Surg Am 2009; 91 (Suppl. 2, Pt. 1):131–138. doi: 10.2106/JBJS.H.01061.

21. Siegmeth A, Duncan CP, Masri BA, Kim WY, Garbuz DS. Modular tantalum augments for acetabular defects in revision hip arthroplasty. Clin Orthop Relat Res 2009; 467:199–205. doi: 10.1007/s11999-008-0549-0.

22. Sporer SM, Paprosky WG. The use of a trabecular metal acetabular component and trabecular metal augment for severe acetabular defects. J Arthroplasty 2006; 21:83–86. doi:10.1016/j.arth.2006.05.008.

23. Unger AS, Duggan JP. Midterm results of a porous tantalum monoblock tibia component clinical and radiographic results of 108 knees. J Arthroplasty 2011; 26:855–860. doi: 10.1016/j.arth.2010.08.017.

24. Van Kleunen JP, Lee GC, Lementowski PW, Nelson CL, Garino JP. Acetabular revisions using trabecular metal cups and augments. J Arthroplasty 2009; 24:64–68. doi: 10.1016/j.arth.2009.02.001.

25. Vicario C, Lopez-Oliva F, Sánchez-Lorente T, Zimmermann M, Asenjo-Siguero JJ, Ladero F, et al. Anterior cervical fusion with tantalum interbody implants. Clinical and radiological results in a prospective study [in Spanish]. Neurocirugia (Astur) 2006; 17:132–139. doi:10.1016/S1130-1473(06)70354-2.

26. Høy K, Bünger C, Niederman B, Helmig P, Hansen ES, Li H, et al. Transforaminal lumbar interbody fusion (TLIF) versus posterolateral instrumented fusion (PLF) in degenerative lumbar disorders: a randomized clinical trial with 2-year follow-up. Eur Spine J 2013; 22:2022–2029. doi: 10.1007/s00586-013-2760-2.

27. Lequin MB, Verbaan D, Bouma GJ. Posterior lumbar interbody fusion with stand-alone trabecular metal cages for repeatedly recurrent lumbar disc herniation and back pain. J Neurosurg Spine 2014; 20:617–622. doi: 10.3171/2014.2.SPINE13548.

28. Molloy S, Butler JS, Benton A, Malhotra K, Selvadurai S, Agu O. A new extensile anterolateral retroperitoneal approach for lumbar interbody fusion from L1 to S1: a prospective series with clinical outcomes. Spine J 2016; 16:786–791. doi: 10.1016/j.spinee.2016.03.044.

29. Matejka J, Zeman J, Belatka J. Mid-term results of 360-degree lumbar spondylodesis with the use of a tantalum implant for disc replacement. Acta Chir Orthop Traumatol Cech 2009; 76:388–393. doi:10.1186/1471-2474-10-122.

30. Löfgren H, Engquist M, Hoffmann P, Sigstedt B, Vavruch L. Clinical and radiological evaluation of trabecular metal and the Smith-Robinson technique in anterior cervical fusion for degenerative disease: a prospective, randomized, controlled study with 2-year follow-up. Eur Spine J 2010; 19:464–473. doi: 10.1007/s00586-009-1161-z.

31. Zardiackas LD, Parsell DE, Dillon LD, Mitchell DW, Nunnery LA, Poggie R. Structure, metallurgy, and mechanical properties of a porous tantalum foam. J Biomed Mater Res 2001; 58:180–187. doi:10.1002/1097-4636(2001)58:2<180::aid-jbm1005>3.0.co;2-5.

32. Shimko DA, Shimko VF, Sander EA, Dickson KF, Nauman EA. Effect of porosity on the fluid flow characteristics and mechanical properties of tantalum scaffolds. J Biomed Mater Res B Appl Biomater 2005; 73:315–324. doi:10.1002/jbm.b.30229.

33. Toth JM, Wang M, Estes BT, Scifert JL, Seim HB 3rd, Turner AS. Polyetheretherketone as a biomaterial for spinal applications. Biomaterials 2006; 27:324–334. doi:10.1016/j.biomaterials.2005.07.011.

34. Brantigan JW, Steffee AD. A carbon fiber implant to aid interbody lumbar fusion. Two-year clinical results in the first 26 patients. Spine 1993; 18:2106–2107. doi:10.1007/978-4-431-68234-9_41.

35. Bridwell KH, Lenke LG, McEnery KW, Baldus C, Blanke K. Anterior fresh frozen structural allografts in the thoracic and lumbar spine. Do they work if combined with posterior fusion and instrumentation in adult patients with kyphosis or anterior column defects? Spine 1995; 20:1410–1418. doi:10.1097/00007632-199506020-00014.

36. Hanc M, Fokter SK, Vogrin M, Molicnik A, Recnik G. Porous tantalum in spinal surgery: an overview. Eur J Orthop Surg Traumatol 2016; 26:1–7. doi: 10.1007/s00590-015-1654-x.

37. Levine BR, Sporer S, Poggie RA, Della Valle CJ, Jacobs JJ. Experimental and clinical performance of porous tantalum in orthopedic surgery. Biomaterials 2006; 27:4671–4681. doi:10.1016/j.biomaterials.2006.04.041.

38. Bagby GW. Arthrodesis by the distractive-compression method using a stainless steel implant. Orthopedics 1988; 11:931–934. doi:10.3109/17453678809149379.

39. Kuslich SD, Ulstrom CL, Griffith SL, Ahern JW, Dowdle JD. The Bagby and Kuslich method of lumbar interbody fusion. History, techniques, and 2-year follow-up results of a United States prospective, multicenter trial. Spine 1998; 23:1267–1278. doi:10.1097/00007632-199806010-00019.

40. McAfee PC, Regan JJ, Geis WP, Fedder IL. Minimally invasive anterior retroperitoneal approach to the lumbar spine. Emphasis on the lateral BAK. Spine 1998; 23:1476–1484. doi:10.1097/00007632-199807010-00009.

41. Ray CD. Threaded titanium cages for lumbar interbody fusions. Spine 1997; 22:667–680. doi:10.1097/00007632-199703150-00019.

42. Sandhu HS, Turner S, Kabo JM, Kanim LE, Liu D, Nourparvar A, et al. Distractive properties of a threaded interbody fusion device. An in vivo model. Spine 1996; 21:1201–1210. doi:10.1097/00007632-199605150-00013.

43. Weiner BK, Fraser RD. Spine update: lumbar interbody cages. Spine 1998; 23:634–640. doi:10.1097/00007632-199803010-00020.

44. Cizek GR, Boyd LM. Imaging pitfalls of interbody spinal implants. Spine 2000; 25:2633–2636. doi:10.1097/00007632-200010150-00015.

45. McAfee PC, Boden SD, Brantigan JW, Fraser RD, Kuslich SD, Oxland TR, et al. Symposium: a critical discrepancy-a criteria of successful arthrodesis following interbody spinal fusions. Spine 2001; 26:320–334. doi:10.1097/00007632-200102010-00020.

46. Cho DY, Liau WR, Lee WY, Liu JT, Chiu CL, Sheu PC. Preliminary experience using a polyetheretherketone (PEEK) cage in the treatment of cervical disc disease. Neurosurgery 2002; 51:1343–1349. doi:10.1097/00006123-200212000-00003.

47. Kim KS, Yang TK, Lee JC. Radiological changes in the bone fusion site after posterior lumbar interbody fusion using carbon cages impacted with laminar bone chips: follow-up study over more than 4 years. Spine (Phila Pa 1976) 2005; 30:655–660. doi:10.1097/01.brs.0000155421.07796.7f.

48. Kao TH, Wu CH, Chou YC, Chen HT, Chen WH, Tsou HK. Risk factors for subsidence in anterior cervical fusion with stand-alone polyetheretherketone (PEEK) cages: a review of 82 cases and 182 levels. Arch Orthop Trauma Surg 2014; 134:1343–1351. doi: 10.1007/s00402-014-2047-z.

49. Stein IC, Than KD, Chen KS, Wang AC, Park P. Failure of a polyether-ether-ketone expandable interbody cage following transforaminal lumbar interbody fusion. Eur Spine J 2015; 24 (Suppl. 4): S555–S559. doi: 10.1007/s00586-014-3704-1.

50. Yang JJ, Yu CH, Chang BS, Yeom JS, Lee JH, Lee CK. Subsidence and nonunion after anterior cervical interbody fusion using a stand-alone polyetheretherketone (PEEK) cage. ClinOrthop Surg 2011; 3:16–23. doi: 10.4055/cios.2011.3.1.16.

51. Kieswetter K, Schwartz Z, Dean DD, Boyan BD. The role of implant surface characteristics in the healing of bone. Crit Rev Oral Biol Med 1996; 7:329–345. doi:10.1177/10454411960070040301.

52. Lincks J, Boyan BD, Blanchard CR, Lohmann CH, Liu Y, Cochran DL, et al. Response of MG63 osteoblast-like cells to titanium and titanium alloy is dependent on surface roughness and composition. Biomaterials 1998; 19:2219–2232. doi:10.1016/S0142-9612(98)00144-6.

53. Tang Z, Xie Y, Yang F, Huang Y, Wang C, Dai K, et al. Porous tantalum coatings prepared by vacuum plasma spraying enhance bmscsosteogenic differentiation and bone regeneration in vitro and in vivo. PLoS One 2013; 8:e66263. doi: 10.1371/journal.pone.0066263.
54. Zou X, Li H, Bünger M, Egund N, Lind M, Bünger C. Bone ingrowth characteristics of porous tantalum and carbon fiber interbody devices: an experimental study in pigs. Spine J 2004; 4:99–105. doi:10.1016/s1529-9430(03)00407-8.
55. Huang B, Zou X, Li H, Xue Q, Bünger C. Short-term alendronate treatment does not maintain a residual effect on spinal fusion with interbody devices and bone graft after treatment withdrawal: an experimental study on spinal fusion in pigs. Eur Spine J 2013; 22:287–295. doi: 10.1007/s00586-012-2513-7.
56. Kim KH, Park JY, Chin DK. Fusion criteria for posterior lumbar interbody fusion with intervertebral cages: the significance of traction spur. J Korean Neurosurg Soc 2009; 46:328–332. doi: 10.3340/jkns.2009.46.4.328.
57. McAfee PC. Interbody fusion cages in reconstructive operations on the spine. J Bone Joint Surg Am 1999; 81:859–880. doi:10.1016/S0883-5403(99)90111-0.
58. Togawa D, Bauer TW, Brantigan JW, Lowery GL. Bone graft incorporation in radiographically successful human intervertebral body fusion cages. Spine 2001; 26:2744–2750. doi:10.1097/00007632-200112150-00025.
59. Horowitz SM, Doty SB, Lane JM, Burstein AH. Studies of the mechanism by which the mechanical failure of poly-methylmethacrylate leads to bone resorption. J Bone Joint Surg Am 1993; 75:802–813. doi:10.1016/S0749-8063(05)80434-7.
60. Horowitz SM, Luchetti WT, Gonzales JB, Ritchie CK. The effect of cobalt chromium upon macrophages. J Biomed Mater Res 1998; 41:468–473. doi:10.1002/(sici)1097-4636(19980905)41:3<468::aid-jbm17>3.0.co;2-e.
61. Jiranek WA. Tissue response to particulate polymethylmethacry-late in mice with various immune deficiencies. J Bone Joint Surg Am 1995; 77:1650–1661. doi:10.1111/j.1365-2591.1995.tb00320.x.